How to cite: *Angew. Chem. Int. Ed.* **2022,** *61,* e202202650
International Edition: doi.org/10.1002/anie.202202650
German Edition: doi.org/10.1002/ange.202202650

Oxygen Reduction **Hot Paper**

Molecular Iron Oxide Clusters Boost the Oxygen Reduction Reaction of Platinum Electrocatalysts at Near-Neutral pH

Jia-Qi Lv[+], Zhong-Ling Lang[+], Jia-Qi Fu[+], Qiao Lan, Rongji Liu, Hong-Ying Zang, Yang-Guang Li, Ding-Ding Ye,* and Carsten Streb**

Abstract: The oxygen reduction reaction (ORR) is a key energy conversion process, which is critical for the efficient operation of fuel cells and metal–air batteries. Here, we report the significant enhancement of the ORR-performance of commercial platinum-on-carbon electrocatalysts when operated in aqueous electrolyte solutions (pH 5.6), containing the polyoxoanion $[Fe_{28}(\mu_3\text{-}O)_8(L\text{-}(-)\text{-}tart)_{16}(CH_3COO)_{24}]^{20-}$. Mechanistic studies provide initial insights into the performance-improving role of the iron oxide cluster during ORR. Technological deployment of the system is demonstrated by incorporation into a direct formate microfluidic fuel cell (DFMFC), where major performance increases are observed when compared with reference electrolytes. The study provides the first examples of iron oxide clusters in electrochemical energy conversion and storage.

The oxygen reduction reaction (ORR) is one of the most important chemical reactions. In nature, the ORR is a cornerstone of metabolic cycles and energy exchange, while in electrochemical technologies, it is at the heart of energy conversion/storage systems such as fuel cells[1,2] and metal-air batteries.[3,4] ORR can principally proceed via four proton/four electron reduction (i.e. O_2 to H_2O), or two proton/two electron reduction (O_2 to H_2O_2).[5,6] The second reaction is undesirable, as the reactive peroxide species formed can oxidatively degrade sensitive components within the system.[7]

As the ORR is a complex reaction with rather sluggish kinetics,[8,9] both natural and artificial systems utilize catalysts to enhance the ORR performance.[10,11] In technological settings such as fuel cells, to-date, noble metals such as platinum on carbon (Pt/C) are the most often used catalysts due to their high performance and catalytic efficiency.[1,2] However, the system suffers from several drawbacks.[12,13] From an economic point of view, the high costs associated with Pt metal negatively affect large-scale deployment.[2] Also, aggregation of typical nanostructured Pt nanoparticles as well as Pt-dependent degradation of the carbon electrode are fundamental challenges for long-term operation.[5] In addition, Pt/C does not show good ORR performance in the presence of coordinating anions (e.g. phosphate),[14–16] which are present in many typical proton exchange membrane fuel cells (PEMFCs).[15,17,18] Researchers worldwide are exploring how to overcome these limitations, and approaches range from the use of non-platinum metal ORR catalysts[10] to the design of nanostructured Pt alloys[19] and highly dispersed Pt particles or (sub)monolayers on non-noble metals.[18] In addition, the use of mediators dissolved in the electrolyte has attracted significant attention. This includes redox mediators,[20] proton-transfer mediators[21] as well as mediators which increase O_2 solubility,[22] leading to enhanced electrocatalytic ORR.

Here, we describe a solution-based alternative approach which facilitates enhanced ORR performance while employing widely used commercial Pt/C ORR catalysts: iron oxide polyanions are introduced as redox-mediators into the

[*] Dr. J.-Q. Lv,[+] J.-Q. Fu,[+] Prof. H.-Y. Zang, Prof. Y.-G. Li
Key Lab of Polyoxometalate, Science of Ministry of Education, Key Laboratory of Nanobiosensing and Nanobioanalysis at Universities of Jilin Province, Institute of Functional Material Chemistry, Faculty of Chemistry, Northeast Normal University
Changchun 130024 (China)
E-mail: zanghy100@nenu.edu.cn

Dr. Z.-L. Lang[+]
Centre for Advanced Optoelectronic Functional Materials Research and Key Laboratory for UV Light-Emitting Materials and Technology of Ministry of Education, Northeast Normal University, Changchun 130024 (China)

Dr. Q. Lan, Prof. Dr. D.-D. Ye
Institute of Engineering Thermophysics, School of Energy and Power Engineering, Chongqing University
No. 174 Shazheng Street, Shapingba District, Chongqing 400030 (China)
E-mail: dingdingye@cqu.edu.cn

Dr. R. Liu, Prof. C. Streb
Institute of Inorganic Chemistry I, Ulm University
Albert-Einstein-Allee 11, 89081 Ulm (Germany)

Dr. R. Liu, Prof. C. Streb
Helmholtz-Institute Ulm (HIU)
Helmholtzstr. 11, 89081 Ulm (Germany)

Prof. C. Streb
Department of Chemistry, Johannes Gutenberg University Mainz
Duesbergweg 10-14, 55131 Mainz (Germany)
E-mail: carsten.streb@uni-mainz.de

[+] These authors contributed equally to this work.

aqueous electrolyte, and experiment and theory suggest that these species enhance ORR at the electrolyte-catalyst interface.

This approach is inspired by pioneering works from the groups of Brechin,[23–26] Cronin,[23–25] Nyman,[27–29] Powell,[30] Wang[31] and others, who discovered that high nuclearity iron oxide polyions with nuclearities ranging from $\{Fe_{13}\}$ to $\{Fe_{34}\}$ can be accessed and stabilized using terminal carboxylate,[27–29,31] alkoxide[25,26,30] or N-donor ligands.[23,24] resulting in redox-active cluster species.[28] Note that these studies were mainly focused on the design of molecular analogues of iron oxide minerals (e.g. ferrihydrite or magnetite) and exploration of the unique magnetic properties of these clusters. In contrast, very little is known about the redox-activity or (electro-)catalytic properties of this compound class. However, metal oxide clusters are well-known redox-mediators,[32] and have been employed in processes ranging from (photo-)electrochemical water-splitting[33,34] to selective organic transformations,[35] dye-sensitized solar cells[36] and fuel cells.[21]

Here, we use the iron oxo cluster $K_2Na_{18}[Fe_{28}(\mu_3\text{-}O)_8(L\text{-}(-)\text{-tart})_{16}(CH_3COO)_{24}]\cdot 29\,H_2O$ ($=Fe_{28}$, tart = tartrate, Figure 1) which was originally reported by Li, Wang and co-workers.[31] Briefly, Fe_{28} is composed of four identical Fe_7 sub-units linked by L-(−)-tartrate bridging ligands (Figure 1). The cluster is in an all-Fe^{III} electron-configuration, and all iron centers are coordinated octahedrally.

Some of us have recently demonstrated that the cluster is water-soluble resulting in aqueous solutions with near-neutral pH and shows catalase-like redox-activity. Based on these observations, we hypothesized that Fe_{28} could be active as a redox-mediator for the ORR.[37] We demonstrate that aqueous solutions containing Fe_{28} show increased ORR activity when used together with a commercial Pt/C working electrode. Experiment and theory provide initial insights into the function and stability of the cluster, and a preliminary study highlights the superior performance of aqueous Fe_{28} solutions as electrolytes in a direct formate microfluidic fuel cell (DFMFC) when compared with reference phosphate buffer solutions.

Fe_{28} was synthesized as described previously; sample identity and purity were confirmed by powder X-ray diffraction FT-IR spectroscopy and electrospray ionization-ion mobility-mass spectrometry (ESI-IM-MS), see Supporting Information, Figures S1–S3. Dissolution studies show a maximum room-temperature solubility of Fe_{28} in water of $\approx$50 mM (corresponding to $\approx$325 g L^{-1}). Thus, aqueous Fe_{28} solutions can be prepared at concentrations suitable for deployment as redox-mediator in ORR reactions.[21]

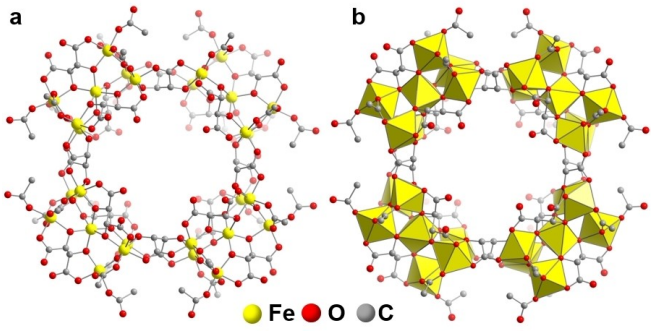

Figure 1. a) Ball-and-stick representation of Fe_{28}. b) Polyhedral representation of Fe_{28}, showing the wheel-like structure assembled from four tartrate-linked Fe_7 building units.

In initial studies, we explored the ORR activity of aqueous solutions containing 0 mM (pH 7.1), 0.5 mM (pH 4.7), 5 mM (pH 5.2) and 50 mM (pH 5.6) Fe_{28} cluster. To this end, we used a three-electrode setup: as working electrode, a glassy carbon rotating disk electrode (operated at 1600 rpm) was modified with Pt/C (20 wt % Pt, loading: 0.20 mg cm^{-2}, details see Supporting Information). A Pt-rod was used as counter electrode, the reference electrode was Ag/AgCl. To facilitate comparison, all potentials were converted to the reversible hydrogen electrode (RHE, see Supporting Information for details).

The system was studied in an electrochemical potential range between $E = 1.1$ V to 0.5 V (vs RHE) using linear sweep voltammetry (LSV). As shown in Figure 2a, the ORR activity of the system increased with increasing Fe_{28} concentration and highest ORR performance was observed in aqueous solutions containing 50 mM Fe_{28}, thus highlighting that Fe_{28} solutions can act as efficient electrolyte solutions for ORR catalysis. Cyclic voltammetry (CV) was used to confirm, that Fe_{28} does not show any redox activity within the ORR potential range studied, i.e., between 1.1 V and 0.5 V vs RHE. The first asymmetric $Fe^{III/II}$ redox couple is observed at significantly more negative potentials ($E_{1/2}$: $\approx$0.2 V vs. RHE), see Figure 2b and Supporting Information, Figure S4. Note that the observe asymmetry of the redox wave could be due to a merging of the iron-based redox-couple with the proton-discharge wave, as reported previously.[38] We note that in the absence of Pt/C, i.e., when using a blank glassy carbon working electrode, Fe_{28}-containing aqueous solutions (50 mM) show no significant ORR activity (Figure 2c); however, the Pt/C catalyst in Fe_{28} solution shows a distinct ORR peak at $\approx$0.88 V vs RHE (Supporting Information, Figure S5), highlighting that the observed ORR reactivity increase shown in Figure 2a is a synergistic effect between the Pt/C catalyst and Fe_{28}.

As briefly described above, the ORR performance of Pt/C in neutral phosphate-buffered aqueous solution (PBS) is affected by Pt-poisoning due to phosphate ion adsorption, so that alternative electrolytes are required, for electrochemical operation of Pt/C systems under (near-)neutral pH conditions.[14–16] To provide initial insights into the performance of Fe_{28} and PBS solutions, we performed comparative LSV analyses of aqueous solutions containing Fe_{28} or phosphate buffer (50 mM, pH 5.6), see Figure 2d and Figure S6. These studies showed more positive onset potentials for the Fe_{28} solution ($E_{onset} = 0.97$ V vs. RHE) compared with the phosphate solution ($E_{onset} = 0.89$ V vs. RHE). Similar trends were observed for the half-wave potentials, $E_{1/2}(Fe_{28}) = 0.84$ V vs. RHE, $E_{1/2}(PBS) = 0.74$ V vs. RHE. Also, Tafel-slope analyses of the system indicated that the Fe_{28} solutions show lower kinetic barriers for ORR

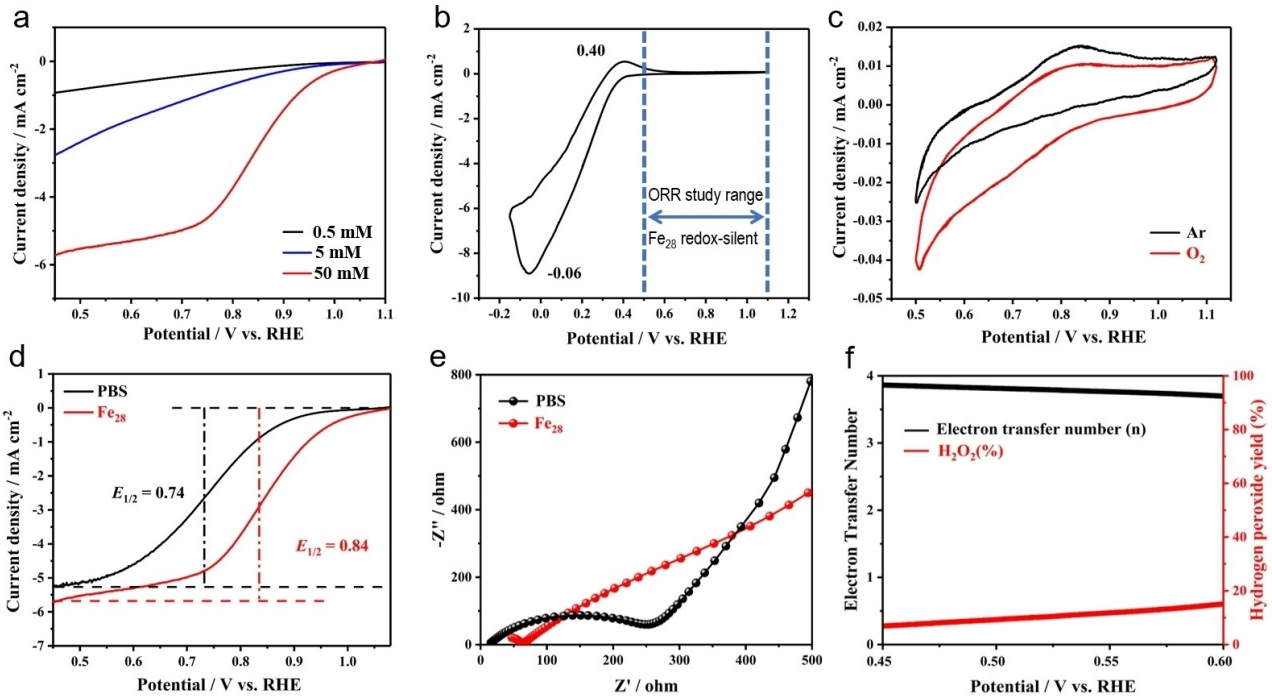

Figure 2. a) RDE-LSV of a Pt/C working electrode in O_2-saturated aqueous solutions containing different amounts of Fe_{28}. b) CV of Ar-saturated aqueous Fe_{28} solution (50 mM) using a non-modified glassy carbon working electrode; note that Fe_{28} is redox-silent in the ORR potential range used for ORR studies (blue dashed lines, 1.1 V to 0.5 V vs. RHE). c) Zoomed-in CV of Fe_{28} (50 mM) in Ar-saturated or O_2-saturated aqueous solution using a non-modified glassy carbon working electrode, showing no significant ORR catalytic current in the presence of oxygen. d) Comparative RDE-LSV analysis of Pt/C (rotation rate 1600 rpm) in oxygen-saturated aqueous solutions containing 50 mM Fe_{28} or 50 mM phosphate buffer. e) Electrochemical impedance spectroscopic (EIS) data of Pt/C in 50 mM aqueous Fe_{28} or PBS solutions. f) Rotating ring-disk electrode (RRDE) voltammetry used to study the selectivity of the ORR; shown are H_2O_2 yield and electron transfer number (n) for a Pt/C working electrode in a 50 mM aqueous Fe_{28} solution.

(106.6 mV dec^{-1}) compared with the PBS solution (136.6 mV dec^{-1}), see Supporting Information, Figure S7. Details on the superior performance of the Fe_{28} electrolyte compared with the reported PBS system are shown in the Supporting Information, Table S1.

Next, we used electrochemical impedance spectroscopy (EIS) to evaluate the charge transfer ability within the systems. As shown in Figure 2e, at open circuit potential, the Nyquist plots for both, the Fe_{28} and the PBS solution show similar overall features with a semicircle in the high-frequency region and a linear slope in the low-frequency domain.[39] The high-frequency data show that the Fe_{28} solution features significantly lower charge-transfer resistance compared to the PBS-containing solution. In contrast, in the low-frequency domain, both Fe_{28} and PBS solutions show semi-infinite diffusion behavior, and lower ionic diffusion resistance is observed for PBS compared with Fe_{28}. This is expected, as Fe_{28} is both higher charged and significantly larger than the phosphate ions.

To study the ORR selectivity, we employed rotating ring-disk electrode-LSV (RRDE-LSV), which allows differentiation between 2-electron and 4-electron reduction of O_2. 4-electron reduction (product: H_2O) is the desired process, resulting in formation of water as product, while 2-electron reduction results in peroxide formation which can trigger component degradation (see above). Here, RRDE-LSV was employed using Pt/C-modified working electrodes operated in 50 mM Fe_{28} solution (Figure 2f). Data analysis based on the ring-current allowed us to determine the H_2O_2 yields and electron transfer numbers n, which is a measure of the selectivity between 2-electron and 4-electron reduction of O_2. As shown in Figure 2f, across the potential range scanned ($E = 0.45$–0.60 V vs RHE), the H_2O_2 yield is $< 20\,\%$, and H_2O_2 formation decreases with decreasing potential. This is also reflected by the electron transfer number n, which increases from $n \approx 3.7$ (0.60 V) to $n \approx 3.9$ (0.45 V), emphasizing the high selectivity for the 4-electron transfer.

Based on these results, we hypothesized that Fe_{28} might affect oxygen uptake and/or oxygen solubility in the aqueous electrolyte as a basis for the enhanced ORR observed. Note that gas uptake by liquids[40] is affected by a variety of factors ranging from gas flow rate to surface tension and ionic strength of the solution.[41] Here, we used time-resolved oxygen sensing[42] to determine O_2-uptake by aqueous solutions of Fe_{28} and PBS (50 mM). To this end, the dissolved O_2 concentration in the aqueous solvent was recorded as a function of time using a fluorescent O_2 sensor.[42] As shown in Figure 3a, under identical experimental conditions, faster O_2 uptake is observed for the Fe_{28} solution (12.6 ± 0.16 μmol L^{-1} s^{-1}) compared with the PBS solution (8.0 ± 0.08 μmol L^{-1} s^{-1}). Both solutions show virtually identical O_2 saturation concentrations (≈ 750 μmol L^{-1}).

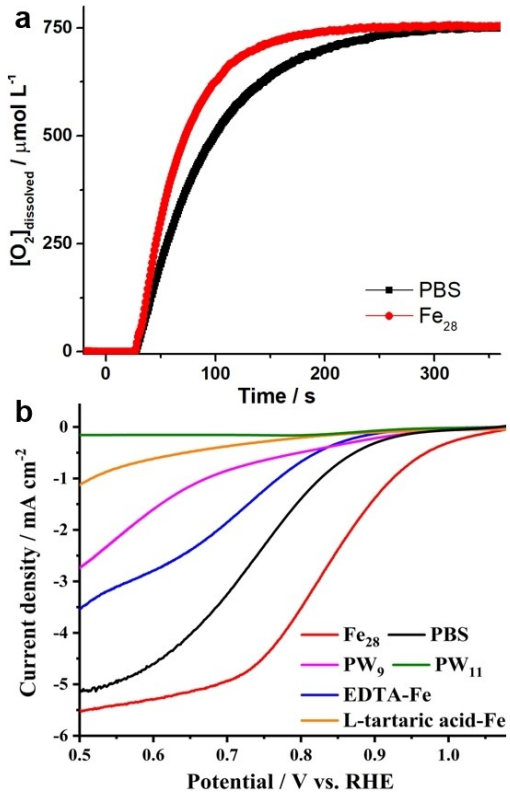

Figure 3. a) Oxygen uptake studies for aqueous solutions of PBS and Fe_{28}. b) LSV of Pt/C at 1600 rpm in aqueous solutions containing 50 mM of PW_{11}, P_2W_{15}, PW_9, PBS and Fe_{28}, EDTA-Fe and L-tartaric acid-Fe.

These results highlight that the presence of Fe_{28} in the aqueous solution improves O_2 uptake rates, and thus mass transfer from the gas to the liquid phase. This could be a main contributor to the enhanced ORR activity.

Next, we were interested whether the observed reactivity enhancement is specific to Fe_{28} or can be triggered by any polyoxoanion. To this end, we performed comparative ORR studies using Pt/C as catalyst in aqueous solutions (50 mM) of the model polyoxoanions $Na_9[A\text{-}PW_9O_{34}]\cdot 7H_2O$ (PW_9) and $Na_7[\alpha\text{-}PW_{11}O_{39}]$ (PW_{11}). As shown in Figure 3b, in all cases, RDE-LSV analyses showed poor ORR performance, thereby highlighting that the observed reactivity enhancement is a Fe_{28}-specific effect. We also examined whether the effect can be reproduced by simple dissolved Fe^{III} species and performed ORR-studies using EDTA/Fe or L-tartrate/Fe complexes ([Fe] = 50 mM, for details see Supporting Information) as electrolyte solutions. As shown in Figure 3b, these systems also showed poor ORR performance, emphasizing that the observed ORR-enhancement is a Fe_{28}-specific effect. For comparison,, we also synthesized two other iron-containing clusters ($Na_4[PW_{11}O_{39}Fe^{III}(H_2O)]$[43] and $Na_3[Bi_6Fe_{13}O_{16}(OH)_{12}(CF_3COO)_{12}](CF_3COO)_4\cdot 36H_2O$,[44] which can be deployed at near-neutral pH according to the literature. CV tests show virtually no enhanced ORR activity under the conditions used for Fe_{28}, which highlights that the observed effects are unique to the Fe_{28} system (details see Supporting Information, Figures S8 and S9).

The stability and recovery of Fe_{28} was studied by analyzing the material after long-time chronoamperometry (CA, $E = 0.84$ V vs RHE, $t_{CA} = 11$ h, Supporting Information, Figure S10), where a near-constant current density was observed, which highlights the robustness of the system. In contrast, the CA of Pt/C in PBS shows significantly lower stability (Supporting Information, Figure S10). The Fe_{28} solutions before and after CA were studied using electrospray-ionization ion-mobility mass-spectrometry (ESI-IM-MS); these analyses showed the presence of Fe_{28} before and after CA: the native Fe_{28} cluster was identified by two characteristic envelopes between 900–1100 m/z (charge: 6−), and 1200–1600 m/z (charge: 5−), see Supporting Information, Figures S3 and S11). For detailed experimental and calculated peak assignments, see Supporting Information, Table S2. Post-CA analysis by ESI-IM-MS shows similar characteristic envelopes, and comparison of the experimental and simulated data verify the integrity of the Fe_{28} in the post-CA solution (Figure S11, for experimental and calculated peak assignments see Table S3). Further, drying of the aqueous Fe_{28} solutions under vacuum allows recovery of the compound, and pXRD (Figure S12) as well as Fourier transform infrared (FTIR) spectroscopy (Figure S13) of the dried sample indicated the structural integrity of the recovered Fe_{28}.

To gain insights into the performance of Fe_{28} solutions in real devices, we undertook a comparative study of Fe_{28} and PBS cathode solutions (50 mM) in a DFMFC (Figure 4a). As anode solutions, we employed aqueous sulfuric acid (1 M) containing HCOOH (2 M), see Figure 4. As cathode, a self-breathing Pt-functionalized gas diffusion electrode (GDE) was employed and was operated in air.[45] Electrochemical performance analysis of the DFMFC indicated, that the system operated with Fe_{28} cathode solution shows significantly higher maximum power densities ($\approx$9.5-fold increase, Figure 4b) as well as higher maximum current density (Fe_{28}: $\approx$66 mA cm^{-2}; PBS: $\approx$10 mA cm^{-2}, Figure 4b) compared with the PBS system. This preliminary study therefore highlights that the fundamental ORR enhancement observed in the initial experimental studies can be transferred to improving the performance of fuel cells on the cell level.

Based on these findings, we were interested to understand whether the ORR enhancement of Fe_{28} is specific to Pt/C, or if it can be generalized to other ORR catalysts. Initial studies were performed using a FeCo alloy ORR catalyst synthesized according to the reported literature,[46] and comparative LSV analyses of the catalyst in aqueous PBS or Fe_{28} solution showed that the ORR-enhancing effect of Fe_{28} is also observed for this system (Figure S14).

Finally, we were interested in providing initial insights into whether iron oxide polyions can in principle be ORR catalysts in their own right. To this end, we performed a series of spin-polarized density functional theory (DFT) calculations to predict the Gibbs free energy changes of the ORR process using a simplified Fe_7 cluster (Figure 5a). This was compared with a three-layer slab model of Pt(111) as

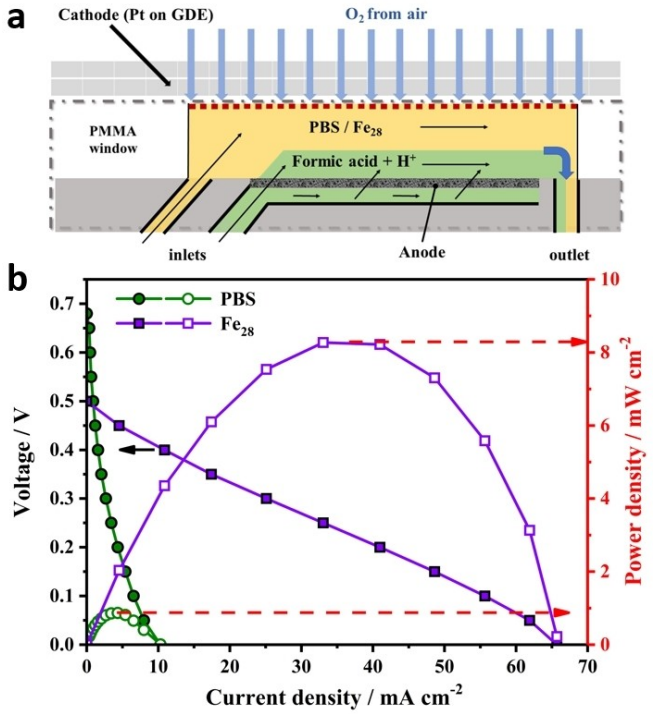

Figure 4. a) Scheme of the direct formate microfluidic fuel cell (DFMFC) used. b) DFMFC cell performance for aqueous PBS or Fe_{28} cathode solutions (50 mM), based on cell voltage (closed symbols) and cell power density (open symbols). Conditions: anode solutions: aqueous H_2SO_4 (1 M) containing HCOOH (2 M). Catalyst loadings: cathode Pt/C (20%), 3.5 mg cm^{-2}; anode: Pd particles, 5 mg cm^{-1}. cathode/anode solution flow rates: 200 µL min^{-1}.

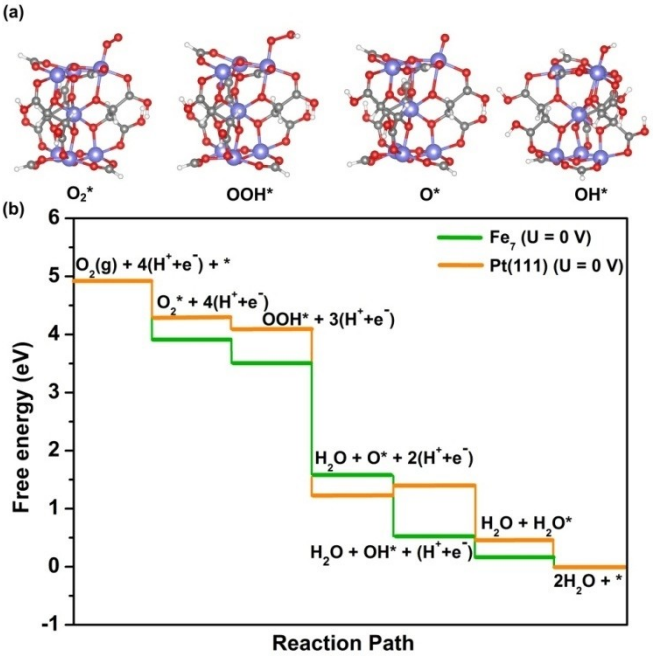

Figure 5. a) The optimized geometric configurations for OH, O, and OOH intermediates bound to the Fe_7 model catalyst. Color code: Fe: blue, C: gray, O: red, H: white. b) The free energy diagrams for ORR on Fe_7 and Pt (111) at 0 V (vs. standard hydrogen electrode, SHE).

benchmark (for details see Supporting Information). Under neutral pH conditions, ORR generally involves four intermediate species, i.e. surface-adsorbed O_2*, OOH*, O*, and OH*. Thus, moderate free energies of adsorption for these intermediates are crucial in determining the catalytic efficiency. Figure 5b illustrates the Gibbs free energy diagrams for ORR by Fe_7 and the Pt(111) surface calculated based on the theoretical framework developed by Nørskov et al.[5] Our initial data suggest that O_2 adsorption on Fe_7 is 0.37 eV more favorable than on the classical Pt(111), suggesting that iron oxo clusters might be acting as active oxygen transporters for ORR reactions. The following ORR reaction steps proceed energetically downhill, and desorption of OH* is determined as the rate-limiting step. This initial theoretical analysis suggests that future experimental studies on the use iron oxide clusters as ORR catalysts are warranted and could lead to new, noble metal-free molecular ORR catalysts.

In sum, we present the first example of the use of molecular iron oxide clusters as soluble enhancers for electrocatalytic reactions. Solutions containing the high-nuclearity Fe_{28} iron oxide cluster show synergistic enhancement of the oxygen reduction reaction when operated with standard Pt/C catalysts in aqueous solution at near-neutral pH. Initial mechanistic studies suggest that the Fe_{28} solutions allow improved O_2 mass transport from the gas phase to the liquid phase and on to the solid Pt/C catalyst. Comparative studies with a FeCo alloy ORR catalyst show that this catalytic performance improvement of Fe_{28} can be generalized to other ORR catalyst classes. The results obtained from principal electrochemical studies were transferred to the device level and showed significantly improved performance when operated in a direct formate microfluidic fuel cell. Future work will study the role of Fe_{28} under operating conditions to gain further experimental and theoretical insights into the mechanism of reactivity enhancement.

Acknowledgements

This work was financially supported by the National Natural Science Foundation of China (Grant No. 21871042, 21471028, 21673098, 21671036), Natural Science Foundation of Jilin Province (Grant No. 20200201083JC), Jilin Provincial Education Department (Grant No. JJKH20201169KJ), the Fundamental Research Funds for the Central Universities (Grant No. 2412015KJ012, 2412017BJ004). R.L. acknowledges the Alexander-von-Humboldt Foundation for financial support. C.S. and R.L. acknowledge Ulm University, Johannes Gutenberg University Mainz, the Gutenberg Research College (Mainz), SusInnoScience (Mainz) and the Helmholtz-Gemeinschaft HGF for support. C.S. acknowledges the Deutsche Forschungsgemeinschaft DFG (STR1164/12, Collaborative Research Center TRR234 "CataLight", Project No: 364549901) for financial support. Open Access funding enabled and organized by Projekt DEAL.

Conflict of Interest

The authors declare no conflict of interest.

Data Availability Statement

The data that support the findings of this study are available from the corresponding author upon reasonable request.

Keywords: Electrocatalysis · Iron Oxide · Oxygen Reduction Reaction · Polyoxometalates · Self-Assembly

[1] S. Zhang, O. Oms, L. Hao, R. Liu, M. Wang, Y. Zhang, H. Y. He, A. Dolbecq, J. Marrot, B. Keita, et al., *ACS Appl. Mater. Interfaces* **2017**, *9*, 38486–38498.
[2] H. A. Gasteiger, N. M. Marković, *Science* **2009**, *324*, 48–49.
[3] J. Zhang, Z. Zhao, Z. Xia, L. Dai, *Nat. Nanotechnol.* **2015**, *10*, 444–452.
[4] G. Yang, J. Zhu, P. Yuan, Y. Hu, G. Qu, B.-A. Lu, X. Xue, H. Yin, W. Cheng, J. Cheng, et al., *Nat. Commun.* **2021**, *12*, 1734.
[5] A. Kulkarni, S. Siahrostami, A. Patel, J. K. Nørskov, *Chem. Rev.* **2018**, *118*, 2302–2312.
[6] Z. Liang, H. Guo, G. Zhou, K. Guo, B. Wang, H. Lei, W. Zhang, H. Zheng, U.-P. Apfel, R. Cao, *Angew. Chem. Int. Ed.* **2021**, *60*, 8472–8476; *Angew. Chem.* **2021**, *133*, 8553–8557.
[7] H. Singh, S. Zhuang, B. Ingis, B. B. Nunna, E. S. Lee, *Carbon* **2019**, *151*, 160–174.
[8] H. A. Gasteiger, S. S. Kocha, B. Sompalli, F. T. Wagner, *Appl. Catal. B* **2005**, *56*, 9–35.
[9] Z.-F. Huang, J. Song, S. Dou, X. Li, J. Wang, X. Wang, *Matter* **2019**, *1*, 1494–1518.
[10] X. Tian, X. F. Lu, B. Y. Xia, X. W. (David) Lou, *Joule* **2020**, *4*, 45–68.
[11] Y.-J. Wang, W. Long, L. Wang, R. Yuan, A. Ignaszak, B. Fang, D. P. Wilkinson, *Energy Environ. Sci.* **2018**, *11*, 258–275.
[12] G. Wu, K. L. More, C. M. Johnston, P. Zelenay, *Science* **2011**, *332*, 443–447.
[13] H. M. A. Amin, U.-P. Apfel, *Eur. J. Inorg. Chem.* **2020**, 2679–2690.
[14] Q. He, B. Shyam, M. Nishijima, D. Ramaker, S. Mukerjee, *J. Phys. Chem. C* **2013**, *117*, 4877–4887.
[15] Q. Li, G. Wu, D. A. Cullen, K. L. More, N. H. Mack, H. T. Chung, P. Zelenay, *ACS Catal.* **2014**, *4*, 3193–3200.
[16] J. M. Falkowski, N. M. Concannon, B. Yan, Y. Surendranath, *J. Am. Chem. Soc.* **2015**, *137*, 7978–7981.
[17] Z. Wen, S. Ci, F. Zhang, X. Feng, S. Cui, S. Mao, S. Luo, Z. He, J. Chen, *Adv. Mater.* **2012**, *24*, 1399–1404.
[18] X. Wang, Z. Li, Y. Qu, T. Yuan, W. Wang, Y. Wu, Y. Li, *Chem* **2019**, *5*, 1486–1511.
[19] C. Cui, L. Gan, M. Heggen, S. Rudi, P. Strasser, *Nat. Mater.* **2013**, *12*, 765–771.
[20] M. Li, X. Bi, R. Wang, Y. Li, G. Jiang, L. Li, C. Zhong, Z. Chen, J. Lu, *Matter* **2020**, *2*, 32–49.
[21] C. W. Anson, S. S. Stahl, *Chem. Rev.* **2020**, *120*, 3749–3786.
[22] Q. Yang, Z. Zhang, X.-G. Sun, Y.-S. Hu, H. Xing, S. Dai, *Chem. Soc. Rev.* **2018**, *47*, 2020–2064.
[23] A. E. Dearle, D. J. Cutler, M. Coletta, E. Lee, S. Dey, S. Sanz, H. W. L. Fraser, G. S. Nichol, G. Rajaraman, J. Schnack, et al., *Chem. Commun.* **2022**, *58*, 52–55.
[24] A. E. Dearle, D. J. Cutler, H. W. L. Fraser, S. Sanz, E. Lee, S. Dey, I. F. Diaz-Ortega, G. S. Nichol, H. Nojiri, M. Evangelisti, et al., *Angew. Chem. Int. Ed.* **2019**, *58*, 16903–16906; *Angew. Chem.* **2019**, *131*, 17059–17062.
[25] D. J. Cutler, M. K. Singh, G. S. Nichol, M. Evangelisti, J. Schnack, L. Cronin, E. K. Brechin, *Chem. Commun.* **2021**, *57*, 8925–8928.
[26] G. W. Powell, H. N. Lancashire, E. K. Brechin, D. Collison, S. L. Heath, T. Mallah, W. Wernsdorfer, *Angew. Chem. Int. Ed.* **2004**, *43*, 5772–5775; *Angew. Chem.* **2004**, *116*, 5896–5899.
[27] O. Sadeghi, L. N. Zakharov, M. Nyman, *Science* **2015**, *347*, 1359–1362.
[28] O. Sadeghi, C. Falaise, P. I. Molina, R. Hufschmid, C. F. Campana, B. C. Noll, N. D. Browning, M. Nyman, *Inorg. Chem.* **2016**, *55*, 11078–11088.
[29] O. Sadeghi, M. Amiri, E. W. Reinheimer, M. Nyman, *Angew. Chem. Int. Ed.* **2018**, *57*, 6247–6250; *Angew. Chem.* **2018**, *130*, 6355–6358.
[30] A. K. Powell, S. L. Heath, D. Gatteschi, L. Pardi, R. Sessoli, G. Spina, F. Del Giallo, F. Pieralli, *J. Am. Chem. Soc.* **1995**, *117*, 2491–2502.
[31] Z.-M. Zhang, Y.-G. Li, S. Yao, E.-B. Wang, Y.-H. Wang, R. Clérac, *Angew. Chem. Int. Ed.* **2009**, *48*, 1581–1584; *Angew. Chem.* **2009**, *121*, 1609–1612.
[32] N. Li, J. Liu, B.-X. Dong, Y.-Q. Lan, *Angew. Chem. Int. Ed.* **2020**, *59*, 20779–20793; *Angew. Chem.* **2020**, *132*, 20963–20977.
[33] B. Rausch, M. D. Symes, G. Chisholm, L. Cronin, *Sci. J.* **2014**, *345*, 1326–1330.
[34] L. G. Bloor, R. Solarska, K. Bienkowski, P. J. Kulesza, J. Augustynski, M. D. Symes, L. Cronin, *J. Am. Chem. Soc.* **2016**, *138*, 6707–6710.
[35] A. D. Stergiou, M. D. Symes, *Catal. Today* **2022**, *384–386*, 146–155.
[36] T. M. A. Bakker, S. Mathew, J. N. H. Reek, *Sustainable Energy Fuels* **2019**, *3*, 96–100.
[37] M.-J. Wei, J.-Q. Fu, B. Li, K.-Z. Shao, H.-Y. Zang, X.-H. Wang, Z.-M. Su, *New J. Chem.* **2019**, *43*, 13430–13436.
[38] A. Dolbecq, J. D. Compain, P. Mialane, J. Marrot, F. Sécheresse, B. Keita, L. R. B. Holzle, F. Miserque, L. Nadjo, *Chem. Eur. J.* **2009**, *15*, 733–741.
[39] C. Brett, A. M. Oliveira Brett, *Electrochemistry: Principles, Methods, and Applications*, Oxford University Press, Oxford, **1993**.
[40] M. Lechner, R. Güttel, C. Streb, *Dalton Trans.* **2016**, *45*, 16716–16726.
[41] P. K. Weissenborn, R. J. Pugh, *J. Colloid Interface Sci.* **1996**, *184*, 550–563.
[42] F. L. Huber, S. Amthor, B. Schwarz, B. Mizaikoff, C. Streb, S. Rau, *Sustainable Energy Fuels* **2018**, *2*, 1974–1978.
[43] Y. Hua, C. Wang, H. Duan, Q. Xu, T. Peng, D. Yu, X. Xu, X. Liu, *Electrochim. Acta* **2011**, *58*, 99–104.
[44] B. Kandasamy, E. Lee, D.-L. Long, N. Bell, L. Cronin, *Inorg. Chem.* **2021**, *60*, 14772–14778.
[45] T. Zhang, X. Zhu, D.-D. Ye, R. Chen, Y. Zhou, Q. Liao, *Nanoscale* **2020**, *12*, 20270–20278.
[46] C. Li, M. Wu, R. Liu, *Appl. Catal. B* **2019**, *244*, 150–158.

Manuscript received: February 17, 2022
Accepted manuscript online: April 5, 2022
Version of record online: April 21, 2022